A numerical scheme for modeling wavefront propagation on a monolayer of arbitrary geometry

S. Zozor[1,5], O. Blanc[1], V. Jacquemet[1], N. Virag[1,3], J.-M. Vesin[1], E. Pruvot[2], L. Kappenberger[2] and C. Henriquez[2,4]

[1] *Signal Processing Institute, EPFL, CH-1015 Lausanne, Switzerland*
[2] *Division of Cardiology, CHUV, CH-1011 Lausanne, Switzerland*
[3] *Medtronic Europe SA, CH-1131 Tolochenaz, Switzerland*
[4] *Department of Biomedical Engineering, Duke University, Durham, NC 27708-0281 USA*
[5] *Laboratoire des Images et des Signaux, Domaine Universitaire, 38402 Saint Martin d'Hères, France*

Published in IEEE Trans. Biomed. Eng. (2003), vol. 50, no. 4, pp. 412-420
http://dx.doi.org/10.1109/TBME.2003.809505

Abstract

The majority of models of wavefront propagation in cardiac tissue have assumed relatively simple geometries. Extensions to complicated three–dimensional representations are computationally challenging due to issues related to both problem size and the correct implementation of flux conservation. In this paper, we present a generalized finite difference scheme (GDFS) to simulate the reaction–diffusion system on a 3D monolayer of arbitrary shape. GDFS is a vertex–centered variant of the finite–volume method that ensures local flux conservation. Owing to an effectively lower dimensionality, the overall computation time is reduced compared to full 3D models at the same spatial resolution. We present the theoretical background to compute both the wavefront conduction and local electrograms using a matrix formulation. The same matrix is used for both these quantities. We then give some results of simulation for simple monolayers and complex monolayers resembling a human atria.

Keywords

Atrial modeling, cardiac propagation, finite difference methods, triangular mesh.

I. Introduction

MOST models of wavefront propagation in cardiac tissue have assumed relatively simple one and two–dimensional geometries, such as lines or rectangular sheets. Full three–dimensional representations are becoming more common [14], using numerical methods such as finite element methods (FEM) or finite volume methods (FVM). Although a more realistic representation of cardiac muscle, three–dimensional models are computationally challenging. A hybrid approach is to simulate the reaction–diffusion system on a 3D monolayer or shell [2], [17]. The advantage of a reduced three–dimensional geometry is that it is possible to simulate complex dynamics with higher spatial resolutions given the reduced number of nodes needed to represent a surface compared to a volume.

Computing scalar fields in complex discrete structures is of course not a new topic. FEM and FVM have been developed to efficiently solve these problems in a wide range of engineering applications. Both methods have been used in cardiac modeling [13], [16], [23], [25]. Recently, Zemlin

et al. used a modified FVM for an extended monolayer atrial model [29], although sparse details of the method and implementation were provided. Shao et al. used a vertex–centered FVM on two–dimensional sheets of simulated cardiac tissue [24]. Alternative formulations of the FVM relying on very simple geometrical concepts have been proposed for heat transfer computations in isotropic 2D materials in unstructured triangular meshes under the name of Direct Finite Difference Method (DFDM) [20], [22].

In this paper, we present a Generalized Finite Difference Scheme (GFDS) for triangular elements that form a 3D shell. The method is a vertex–centered variant of the FVM that ensures local and global flux conservations and allows for spatial variations in tissue properties. We present the theoretical background for the method and an approach for practical implementations for both wavefront conduction and the computation of secondary quantities such as local electrograms.

II. Model of electrical propagation

Cardiac tissue can be represented as a continuous bidomain where properties can be independently assigned to the intracellular (int) and interstitial (ext) spaces [15]. The bidomain model can be written as

$$\begin{cases} \dfrac{1}{S_v}\nabla\cdot(\mathbf{D}_{\text{int}}\,\nabla V_{\text{int}}) &= I_{\text{m}} \\ \\ \dfrac{1}{S_v}\nabla\cdot(\mathbf{D}_{\text{ext}}\,\nabla V_{\text{ext}}) &= -I_{\text{m}} \end{cases} \tag{1}$$

where V_{int} is the intracellular potential, V_{ext} is the interstitial potential, $\mathbf{D}_{\text{int}}$ and $\mathbf{D}_{\text{ext}}$ are the intra and extra cellular conductivity tensors, respectively, S_v is the surface to volume ratio, and I_{m} is the membrane current per unit area that is a function of the transmembrane potential $V_{\text{m}} = V_{\text{int}} - V_{\text{ext}}$. he tissue is assumed to be immersed in a source-free, volume conductor or conducting bath. With the application of the appropriate boundary conditions at the tissue/bath interface, the potential in the bath is assumed to satisfy Laplace's equation. To reduce the computational cost of solving both the bidomain equations (1) and the field potential in the bath, we assume that

- the tissue is thin and lies in an extensive bath,

- the extracellular potential is sufficiently small such that intracellular potential is approximately equal to the transmembrane potential,
- the effect of the extracellular potential on the transmembrane current sources is small such that the bidomain equations can be decoupled.

Under these assumptions, cardiac tissue can be described by a monodomain equation given by

$$\frac{1}{S_v}\nabla \cdot (\mathbf{D}\,\nabla V_{\mathrm{m}}) = C_m \frac{\partial V_{\mathrm{m}}}{\partial t} + (I_{\mathrm{ion}} - I_{\mathrm{stim}}) \tag{2}$$

where the membrane current $I_{\mathrm{m}} = C_m \frac{\partial V_{\mathrm{m}}}{\partial t} + I_{\mathrm{ion}} - I_{\mathrm{stim}}$ is the sum of the current due to the membrane capacitance C_m, the sum of the ionic currents I_{ion} (depending on the ionic model [1], [3], [4], [5], [18], [19]), and I_{stim} is the stimulus current. The conductivity tensor $\mathbf{D}$ is equal to $\mathbf{D}_{\mathrm{int}}$, with the sub-index being discarded for readability purposes. The monodomain equation can alo be viewed as a special case of the bidomain under the conditions when the anisotropy in the intracellular space and interstitial space is equal.

In contrast to the bidomain equations, the monodomain equation (2) does not explicitly compute the intracellular and extracellular potentials, but rather their difference, the transmembrane potential. The potential in the surrounding bath can be estimated, however, by computing the transmembrane current density at each point in the tissue and summing the potential fields generated by each current source. Despite the limitations of the monodomain formulation [15], this estimate should be similar for thin tissue to that obtained with a full bidomain model [8].

III. Cardiac Tissue as a Monolayer

Bidomain and monodomain models can be constructed in one, two and three dimensions. In this paper, we assume that the part of the cardiac anatomy we are modeling is thin enough to be considered as monolayer but not necessarily planar (i.e. can be a surface). The tissue thickness is also assumed to be constant over the whole surface. The surface mesh is constructed as a set of triangles. The extension of the monolayer model to represent three-dimensional objects helps to remove the restrictions imposed by no flux boundaries on the outer edges of planar sheet models,

and thus allows the investigation of the dynamics of interacting wavefronts on a closed surface with internal obstacles. The method also could be useful for studying propagation in thin walled hearts (e.g., the mouse). While not presented here, the GFDS can be extended into full three-dimensions using tetrahedral elements to model thicker tissue.

Using a mesh of triangles, each vertex node corresponds to a cell that *reacts* through current fluxes across the membrane and *diffuses* currents to its neighbors. The use of the vertex–centered, rather than a element–centered approach simplifies the assignment of neighbors of a given node and ensures flux conservation even if some nodes are at a no–flux boundary (e.g. an internal hole).

A. Generalized Finite Difference Scheme

A.1 Divergence theorem

Using the mesh of triangles, a Generalized Finite Difference Scheme (GFDS) can be applied to solve the reaction–diffusion system numerically [6]. To create the discretized form of Equation (2), the divergence theorem is applied. Let I denote the node at which the potential $V_i(t)$ is computed at the time t, where i is the index of node I (in the following, index m is omitted for sake of simplicity). Consider a closed contour $\mathcal{C}_i$, on the surface that defines a piece of surface Ω_i that includes node I (see Figure 1A). For a given vector field $\mathbf{x}$, the divergence theorem yields $\int_{\Omega_i} \nabla \cdot \mathbf{x}\, \mathrm{d}\Omega = \int_{\mathcal{C}_i} \mathbf{x}^t \mathbf{n}\, \mathrm{d}\mathcal{C}$ where ^{t} denotes the transpose (i.e. $\mathbf{x}^t\mathbf{n}$ is the scalar product between $\mathbf{x}$ and $\mathbf{n}$). Using the divergence theorem of Equation (2) yields

$$\frac{1}{S_v} \int_{\mathcal{C}_i} (\mathbf{D}\, \nabla V)^t\, \mathbf{n}\, \mathrm{d}\mathcal{C} = \int_{\Omega_i} \left(C_m \frac{\partial V}{\partial t} + I_{\mathrm{ion}} - I_{\mathrm{stim}} \right) \mathrm{d}\Omega \tag{3}$$

for any node I. Assuming $\frac{\partial V}{\partial t}$, I_{ion} and I_{stim} are constant on surface Ω_i (valid if the surface area is small) then Equation (3) becomes

$$\frac{1}{S_v} \int_{\mathcal{C}_i} (\mathbf{D}\, \nabla V)^t\, \mathbf{n}\, \mathrm{d}\mathcal{C} = \Omega_i \left(C_m \frac{\partial V_i}{\partial t} + I_{\mathrm{ion},i} - I_{\mathrm{stim},i} \right) \tag{4}$$

Replacing the continuous–time derivative of the potential by a finite time–difference $\frac{\partial V_i}{\partial t} \approx \frac{V_i(t+\delta t) - V_i(t)}{\delta t}$ and assuming $I_{\mathrm{ion},i}$ (and $I_{\mathrm{stim},i}$) and the flux (integral term) constant during a time

step we finally obtain the equation

$$V_i(t+\delta t) = V_i(t) + \frac{\delta t}{S_v C_m \Omega_i} \int_{\mathcal{C}_i} (\mathbf{D}\,\nabla V_i(t))^t\,\mathbf{n}\,\mathrm{d}\mathcal{C} \;-\; \frac{\delta t}{C_m}\left(I_{\mathrm{ion},i}(t) - I_{\mathrm{stim},i}(t)\right) \tag{5}$$

A.2 Choice of the contour

To obtain a solution of Equation (5), we must define the contour C_i. Let J (index j) denote a neighboring node of node I and let $\mathcal{N}_i$ denote the ensemble of indices forming the neighborhood of node I. Let K (index k) denote a neighboring node of node I that is also connected to J (i.e. k is in $\mathcal{N}_i \cap \mathcal{N}_j$; and $\mathcal{N}_i \cap \mathcal{N}_j$ usually contains two points, see Figure 1). Let $G_{i,j,k}$ denote the center of gravity of the triplet (I, J, K) and let $M_{i,j}$ denote the midpoint of the doublet (I, J). Using this geometry, the contour can be defined to be formed by the segments $[G_{i,j,k}, M_{i,j}]$ for all $j \in \mathcal{N}_i$ and $k \in \mathcal{N}_i \cap \mathcal{N}_j$ as shown in Figure 1B–D. This choice of the contour has the advantage that is always contained in the meshed surface and provides a complete tessellation of the domain. Furthermore, the gradient is defined on the triangle (I, J, K) at the center of gravity. For each segment $[G_{i,j,k}, M_{i,j}]$ the normal is denoted by $\mathbf{n}_{i,j,k}$ as shown in Figure 1C.

Using the above definition of the contour, Equation (5) can be expressed as

$$V_i(t+\delta t) = V_i(t) + \left(\frac{\delta t}{S_v C_m \Omega_i} \sum_{j \in \mathcal{N}_i} \sum_{k \in \mathcal{N}_i \cap \mathcal{N}_j} \int_{[G_{i,j,k}, M_{i,j}]} (\mathbf{D}\nabla V_i(t))^t\,\mathbf{n}_{i,j,k}\,\mathrm{d}\mathcal{C} \right) - \frac{\delta t}{C_m}\left(I_{\mathrm{ion},i}(t) - I_{\mathrm{stim},i}(t)\right) \tag{6}$$

When defining the contours, two special cases can arise. The first case involves the treatment of holes in the surface, where nodes are defined at the boundary (i.e. the contour is not closed, Figure 2A). The second case involves geometries where several surfaces are connected (e.g. the septum–like structure formed by two adjoined surfaces, see Figure 2B). In the GFDS, holes are equivalent to boundaries such that no current flows from the node into the hole (i.e. no flux). In this case, only one neighbor $K \in \mathcal{N}_i \cap \mathcal{N}_j$ is connected to the neighbor $J \in \mathcal{N}_i$, as illustrated in Figure 2. In the case of N connected surfaces Ω_i^1 to Ω_i^N, it is necessary to consider the fluxes at the union of these surfaces. As shown in Figure 2, there can be three neighbors K_1, K_2 and K_3 in $\mathcal{N}_i \cap \mathcal{N}_j$ connected to the neighbor $J \in \mathcal{N}_i$. Note that using an element–centered approach, these

cases would require either the inclusion of fictitious nodes or some manipulation of the governing equation to ensure the flux conservation.

A.3 Creation of the Weight Matrix

Using Equation (6), where the gradient is evaluated (appendix A), the flux normal to all the contour patches can be determined for a given point I as a weighted sum. Equation (6) can be written compactly as

$$V_i(t+\delta t) = V_i(t) + \frac{\delta t}{S_v C_m} \sum_{j \in \mathcal{N}_i} w_{i,j} \, (V_j(t) - V_i(t)) \; - \; \frac{\delta t}{C_m} \left(I_{\text{ion},i}(t) - I_{\text{stim},i}(t)\right) \tag{7}$$

where the weights $w_{i,j}$, for $j \in \mathcal{N}_i$, are given by

$$w_{i,j} = \frac{1}{2\,\Omega_i} \sum_{k \in \mathcal{N}_i \cap \mathcal{N}_j} \frac{\left(s_{i,k,k}\,\mathbf{v}_{i,j}^t - s_{i,j,k}\,\mathbf{v}_{i,k}^t\right) \mathbf{D}^t \left(\left(s_{i,k,k} - s_{i,j,k}\right)\mathbf{v}_{i,j} + \left(s_{i,j,j} - s_{i,j,k}\right)\mathbf{v}_{i,k}\right)}{\Delta_{i,j,k}^{\frac{3}{2}}} \tag{8}$$

where

$$\begin{cases} s_{i,j,k} \;=\; \mathbf{v}_{i,j}^t \mathbf{v}_{i,k} \qquad s_{i,j,j} = ||\mathbf{v}_{i,j}||^2 \qquad s_{i,k,k} = ||\mathbf{v}_{i,k}||^2 \\ \\ \Delta_{i,j,k} \;=\; s_{i,j,j}s_{i,k,k} - s_{i,j,k}^2 = ||\mathbf{v}_{i,j} \wedge \mathbf{v}_{i,k}||^2 \end{cases} \tag{9}$$

and where the surface Ω_i is the sum of all the sub–surfaces $\Omega_{i,j,k}$ defined by (I, J, K) (see Figure 1), surrounding the point I, namely

$$\Omega_i = \sum_{j \in \mathcal{N}_i} \sum_{k \in \mathcal{N}_i \cap \mathcal{N}_j} \Omega_{i,j,k} \qquad \text{where} \qquad \Omega_{i,j,k} = \frac{1}{12} \, ||\mathbf{v}_{i,j} \wedge \mathbf{v}_{i,k}|| \tag{10}$$

$\wedge$ denotes the cross product, $\mathbf{v}_{i,j}$ denotes the vector composed by the points I and J (see Figure 1C). Note that $k \in \mathcal{N}_i \cap \mathcal{N}_j$ denotes the nodes connected to node J.

The relationship with the classical finite–difference method appears through the finite–difference expression $(V_j(t) - V_i(t))$ of Equation (7).

In the case where $\mathbf{D}$ is not the same at each point, the same equation can be applied except that the tensor $\mathbf{D}$ is replaced by the tensors $\mathbf{D}_{i,j,k}$, defined for a triangle.

The weights $w_{i,j}$ for $j \in \mathcal{N}_i$ form a sparse matrix $\mathbf{W}$, heretofore referred to as the "weight

matrix". Let $\mathbf{P}$ be given by

$$\mathbf{P} = \mathbf{I} + \frac{\delta t}{S_v C_m}(\mathbf{W} - \mathrm{diag}(\mathbf{W}\mathbf{1})) \tag{11}$$

where $\mathbf{I}$ is the identity matrix, $\mathbf{1}$ the vector having 1's for entries and where $\mathrm{diag}(\mathbf{x})$ is the diagonal matrix having the entries x_i of vector $\mathbf{x}$ on the diagonal. Matrix $\mathbf{P}$ is heretofore referred to as the "propagation matrix". Using $\mathbf{P}$, Equation (7) can be written simply in matrix form

$$\mathbf{V}(t+\delta t) = \mathbf{P}\mathbf{V}(t) \; - \; \frac{\delta t}{C_m}\left(\mathbf{I}_{\mathrm{ion}}(t) - \mathbf{I}_{\mathrm{stim}}(t)\right) \tag{12}$$

where $\mathbf{V}$, $\mathbf{I}_{\mathrm{ion}}(t)$ and $\mathbf{I}_{\mathrm{stim}}(t)$ are all vectors.

In this form, the term corresponding to diffusion is replaced by a simple matrix–vector product. Since matrix $\mathbf{P}$ is completely time–independent, it only needs to be calculated once. Note that the weight matrix $\mathbf{W}$ only depends on the diffusion tensor and the geometry. It is clear that the eigenvalues λ_l of the propagation matrix are linked to the eigenvalues $\theta_l^{(w)}$ of matrix $\mathbf{W} - \mathrm{diag}(\mathbf{W}\mathbf{1})$ as follows

$$\lambda_l = 1 + \frac{\delta t}{S_v C_m}\,\theta_l^{(w)} \tag{13}$$

Since $(\mathbf{W} - \mathrm{diag}(\mathbf{W}\mathbf{1}))\,\mathbf{1} = \mathbf{0}$, then $\lambda = 1$ is an eigenvalue of $\mathbf{P}$ that ensures the steady state rest potential on the whole tissue is a solution of the discretized propagation equation. This fact is an obvious consequence of the flux conservation property.

In the case of homogeneous and isotropic diffusion, $\mathbf{D} = \frac{1}{\rho}\mathbf{I}$, the resistivity ρ can be extracted from the weights (appendix F) and the discrete equation is given by

$$V_i(t+\delta t) = V_i(t) + \frac{\delta t}{\rho S_v C_m}\sum_{j\in\mathcal{N}_i} z_{i,j}\;\left(V_j(t) - V_i(t)\right) \; - \; \frac{\delta t}{C_m}\left(I_{\mathrm{ion},i}(t) - I_{\mathrm{stim},i}(t)\right) \tag{14}$$

where the weights $z_{i,j}$, for $j \in \mathcal{N}_i$, are given by

$$z_{i,j} = \frac{1}{2\,\Omega_i}\sum_{k\in\mathcal{N}_i\cap\mathcal{N}_j} \mathrm{cotan}(\vartheta_{i,j,k}) \tag{15}$$

where $\vartheta_{i,j,k}$ is the geometric angle between vectors $\mathbf{v}_{k,i}$ and $\mathbf{v}_{k,j}$ (see Figure 1D) and where the surfaces Ω_i are still defined by (10). Including the weights in matrix $\mathbf{Z}$, the propagation matrix for

the isotropic case is

$$\mathbf{P} = \mathbf{I} + \frac{\delta t}{\rho S_v C_m}(\mathbf{Z} - \mathrm{diag}(\mathbf{Z1})) \tag{16}$$

Matrix $\mathbf{Z}$ depends only on the geometry. Because the eigenvalues of the propagation matrix can then be expressed from the terms of $\mathbf{Z}$ (i.e. $\theta_l^{(z)}$) as

$$\lambda_l = 1 + \frac{\delta t}{\rho S_v C_m}\,\theta_l^{(z)} \tag{17}$$

it is clear that the triangular mesh itself impacts the stability of the part of the algorithm related to diffusion. Notice that matrix $\mathbf{Z} - \mathrm{diag}(\mathbf{Z1})$ is not symmetric since the elements forming the surface are not the same. Considering the diagonal matrix $\mathbf{\Delta}_\Omega = \mathrm{diag}(\ldots, \Omega_i \ldots)$ of the surfaces, however, matrix $\mathbf{Z} - \mathrm{diag}(\mathbf{Z1})$ can be written as the product of $\mathbf{\Delta}_\Omega^{-1}$ and a symmetric matrix. It can then be shown that the eigenvalues of the symmetric matrix are the same as that of matrix $\mathbf{Z} - \mathrm{diag}(\mathbf{Z1})$. This fact implies that the eigenvalues of $\mathbf{Z} - \mathrm{diag}(\mathbf{Z1})$ are real. Now, if one of the $\theta_l^{(z)}$ is positive over the physiological range of parameters and for all time steps, the part of the algorithm corresponding to diffusion will not be stable. Furthermore, it is clear that if θ is an eigenvalue of $\mathbf{Z} - \mathrm{diag}(\mathbf{Z1})$ and $\mathbf{x}$ its associated eigenvector, then $\sum_j z_{i,j}(x_j - x_i) = \theta x_i$ for any i. In the non–isotropic case, the diffusion operation is stable if the real part of the eigenvalues $\theta_l^{(w)}$ are non–positive. A lot of useful theorem on matrices can be found in [12], [27] to study the stability of the propagation matrix.

B. Modeling Electrograms

As noted earlier, the monodomain model can be used to estimate the potentials in the bath by assuming a superposition of potential fields from each of the transmembrane current sources [21]. This approach has been used by Spach et al. [26] to compare simulated and experimental signals in thin tissue and more recently by Gima and Rudy in an inhomogeneous cable [10]. In our case, the monopolar transmembrane current sources are assumed to lie at the surface of the tissue.

Let each node I with its associated surface Ω_i represent a possible source of current $-I_{\mathrm{m},i} S_v\, d$ with d the thickness of the tissue. Following the approach used by Plonsey [21], the bath potential

Φ_E measured by an electrode located at some point E is given by

$$\Phi_E = \frac{1}{4\pi\sigma_0} \int_\Omega \frac{I_\mathrm{m} S_v \, d}{r} \, \mathrm{d}\Omega \tag{18}$$

where r is the distance from the source to the field point and σ_0 is the bath conductivity. Note that the $1/r$ weighting assumes an infinite homogeneous volume conductor. This approximation is used for simplification purposes. It is assumed to be valid since we only simulate local electrograms, where the volume conductor boundary effects and conductor heterogeneities have a reduce impact. A different weighting could be formulated for an inhomogeneous bounded volume conductor using lead field theory.

Assume that r remains constant on the small piece of surface Ω_i surrounding I and thus $r = ||\mathbf{v}_{i,e}||$ the distance between node I and the electrode E. The integration in a general surface is difficult [21]. This assumption, however, is reasonable if the distance from electrode to the surface is greater than the size of the surface. Summing over the entire surface, and assuming again a constant thickness, the potential Φ_E measured on an electrode at position E is given by

$$\Phi_E(t) = \frac{S_v \, d}{4\pi\sigma_0} \sum_i \frac{I_{\mathrm{m},i}(t)}{||\mathbf{v}_{i,e}||} \, \Omega_i \tag{19}$$

Defining the vector of the inverse of the distance from the nodes to the electrode as $\mathbf{ir}_e$ (i.e. the entry i is $\frac{1}{||\mathbf{v}_{i,e}||}$) and the diagonal matrix of the surfaces associated to each node as $\mathbf{\Delta}_\Omega = \mathrm{diag}(\ldots, \Omega_i, \ldots)$, the potential is given by the scalar product

$$\Phi_E(t) = \frac{S_v \, d}{4\pi\sigma_0} \, \mathbf{ir}_e^t \, \mathbf{\Delta}_\Omega \, \mathbf{I}_\mathrm{m}(t) \tag{20}$$

Using the discretized form of the reaction–diffusion equation, the membrane current is equal to the diffusion term. Using the matrix formulation we obtain

$$\Phi_E(t) = \gamma \, \mathbf{ir}_e^t \, \mathbf{\Delta}_\Omega \, (\mathbf{W} - \mathrm{diag}(\mathbf{W1})) \, \mathbf{V}(t) \tag{21}$$

where

$$\gamma = \frac{S_v \, d}{4\pi\sigma_0} \tag{22}$$

Note that the row vector $\gamma\,\mathbf{ir}_e^t\,\mathbf{\Delta}_\Omega\,(\mathbf{W}-\mathrm{diag}(\mathbf{W1}))$ is time–independent and hence, only needs to be calculated once. Several electrograms can also be calculated simultaneously by concatenating several vector $\mathbf{ir}_e$. The formula above is for unipolar signals (i.e. reference at infinity). Bipolar signals can also be calculated by applying superposition and using the vectors given by the two position E and F,

$$\Phi_{E,F}(t) = \gamma\,(\mathbf{ir}_f - \mathbf{ir}_e)^t\,\mathbf{\Delta}_\Omega\,(\mathbf{W}-\mathrm{diag}(\mathbf{W1}))\mathbf{V}(t) \tag{23}$$

C. Results

To demonstrate GFDS for modeling wavefront propagation in cardiac tissue, a two–dimensional 5 cm by 5 cm domain was created. A triangulation was obtained by sub–dividing each square element of a regular, structured grid into two triangles. The internode spacing, $\delta x = \delta y = 400$ μm. The domain was anisotropic, where

$$\mathbf{D} = \frac{1}{\rho}\begin{bmatrix} 1 & 0 \\ 0 & 0.3 \end{bmatrix}, \tag{24}$$

where $\rho = 80$ Ω·cm. A surface to volume ratio of $S_v = 0.24$ $\mu\mathrm{m}^{-1}$ and a specific membrane capacitance of $C_m = 1$ $\mu\mathrm{F}\cdot\mathrm{cm}^{-2}$ were used. A modified Beeler–Reuter model was used to describe the ion fluxes. In the Beeler–Reuter model, the maximum calcium conductance was scaled by 0.9. An explicit Forward Euler time–stepping was used with a time step of $\delta t = 20$ μs. Propagation was initiated by injecting a 80 $\mu\mathrm{A}\cdot\mathrm{cm}^{-2}$ current for 2 ms to a 2 mm^2 area at the center of the sheet.

Figure 3A shows the activation isochrones of the propagating wavefront. The conduction velocity was computed to be 90 $\mathrm{cm}\cdot\mathrm{s}^{-1}$ along the fiber direction and 50 $\mathrm{cm}\cdot\mathrm{s}^{-1}$ across fibers. The ratio of along to across conduction velocities of 1.8 is approximately that predicted by the square root of the ratio of conductivities, $\sqrt{\frac{1}{0.3}} = 1.83$. The advantage of GFDS is that the method can be applied to curved surfaces. Figure 3B shows the activation isochrones of a wavefront propagating on a sphere. The triangulation was obtained by first representing the sphere as an icosahedron. An icosahedron is a surface with 20 faces such that each node is at the same distance to the center and

each face is composed of equilateral triangles. To approximate a sphere, each equilateral triangle is subdivided into 4 triangles using the center of the edge of the initial triangles. The new nodes are then moved in the direction given by the node and the center of the icosahedron, such that they lie on the spherical surface. This process is repeated until the mesh appears sufficiently fine (6 steps in our example). Using this approach a regular mesh can be obtained [11]. The sphere has a radius of 3 cm. The elements comprising the sphere have a mean edge length of 570 μm. Propagation is initiated by injecting a 80 μA$\cdot$cm^{-2} stimulus for 2 ms to a 2 mm^2 area at the top of the sphere. The sphere is composed of 41000 nodes (80000 elements). The parameters are the same as those used for the example above except that the domain is isotropic such that $\mathbf{D} = \frac{1}{\rho}\mathbf{I}$. As shown, the wavefront propagates uniformly on the surface with a conduction velocity of 90 cm$\cdot$s^{-1}.

GFDS can also be applied to general surfaces. Figure 5A shows an atrial geometry obtained from segmentation of an MRI of a human heart. Using custom tools and semi–automated correction, a triangulation was obtained [7]. Note that a Delaunay method for triangulating a general surface does not yet exist. In contrast to the two previous examples, the mesh created for the atria is unstructured.

As seen, the geometry contains holes corresponding to the insertion points of the vessels and location of the valves. In addition, intersecting surfaces of the left and right atrial surfaces form the septum. The mesh has 400'000 nodes (800'000 elements) with a mean size of 200 μm. The propagation was initiated by injecting 80 μA$\cdot$cm^{-2} of current for 2 ms to a 2 mm^2 area near the anatomical location of sinus node.

Figure 5B shows the activation isochrones, revealing a smooth wavefront propagation with a conduction velocity of 88 cm$\cdot$s^{-1}. As noted above, the quality of the mesh is critical to ensure the stability of the diffusion part of the algorithm. Figure 4 shows the effect of the refinement of the mesh. The mesh has to be fine enough to insure minimization of the possible unusual behaviors.

Finally, the matrix formed by GFDS can be used to compute the electrograms near the surface. Because the shape of the electrograms depend in part on the shape of the transmembrane potential,

the Beeler–Reuter model was replaced with the Courtemanche et al. [3] membrane model developed for the human atria. Figure 6 shows the simulated unipolar signals during a sinus like beat at sites E_1 and E_2 (see Figure 5A) located at 1 mm and 5 mm from the atrial surface. Most clinical recordings are bipolar. Figure 7 shows a comparison of simulated bipolar electrograms with 2 mm spacing with those obtained from a decapolar catheter (7 French, BARD catheter with electrode spacing of 2 mm, sampling rate 1 kHz) during routine intracardiac mapping of the atria. Because the properties and conditions in the model and the clinical measurements are not the same, only the shapes are compared, showing excellent agreement.

IV. Concluding remarks

The GFDS using a surface triangular mesh provides a method for studying wavefront conduction on complicated, closed shell structure with uniform thickness. The numerical methods used in this paper are based on local flux conservation, that also guarantees global flux conservation. Other discretization methods like the finite–element formalism, while guaranteeing a global minimization of errors, do not insure the requested local flux conservation in such a straightforward manner.

Our method does not rely on any particular mesh structure, thus easily enabling local mesh refinements if required by local tissue properties, or geometry complexity. Its practical implementation involves the computation of a weight matrix which, for an isotropic homogeneous domain, can be interpreted in terms of the resistive properties of the simulated tissue. This matrix can be precomputed since the material parameters and geometry are typically time and voltage independent: it takes about 24 seconds on a Pentium–IV, 1.8 GHz, for a mesh of 400'000 nodes where each node has at most 10 neighborhoods, to evaluate both the ensembles $\mathcal{N}_i$ for each node I, the intersections $\mathcal{N}_i \cap \mathcal{N}_j$ for each $j \in \mathcal{N}_i$ and then the weights. If the properties or geometry (e.g. due to mechanical contraction) do change, it is possible to compute the matrix as function of time, with an obvious impact on the overall computation time.

We presented here simulation results of sinus rhythm propagation computed with our method

on a realistic human atrial anatomy. A relatively coarse spatial discretization has been used in this example, thus limiting the accuracy of the results. However, further mesh refinements can be used to enhance the accuracy in the same way as they do in the classical forward Finite–Difference Scheme, since both methods rely on the same grounds. Finally, while we present here an explicit formulation in time, the adaptation of this formulation to an implicit scheme is straightforward.

A further interest of the matrix formulation has been illustrated by the computation of secondary quantities such as local electrograms, thus allowing a fast reconstruction of ECG signals. As shown in Figure 6, the shapes of the simulated electrograms are consistent with those obtained experimentally or clinically. The electrograms can be used to further validate models and increase the relevance of the simulated results to clinical measurements.

ACKNOWLEDGMENTS

This study was made possible by grants from the Theo–Rossi–Di–Montelera Foundation, Medtronic Europe, the Swiss Governmental Commission of Inovative Technologies (CTI) and the Swiss National Sciences Foundation (SNSF). The authors wish to thank Ryan Lahm, Drs. Josée Morisette and Arthur Stillman who kindly furnished the atrial geometry surface model. Prof. Craig Henriquez is a Medtronic invited professor at the Division of Cardiology, CHUV.

Appendix

I. Evaluation of the gradient

From the discrete reaction–diffusion Equation (6)

$$V_i(t+\delta t) = V_i(t) + \frac{\delta t}{S_v C_m \Omega_i} \sum_{j \in \mathcal{N}_i} \sum_{k \in \mathcal{N}_i \cap \mathcal{N}_j} \int_{[G_{i,j,k}, M_{i,j}]} (\mathbf{D} \nabla V_i(t))^t \, \mathbf{n} \, \mathrm{d}\mathcal{C} \; - \; \frac{\delta t}{C_m} \left(I_{\mathrm{ion},i}(t) - I_{\mathrm{stim},i}(t) \right)$$

the gradient $\nabla V_i(t)$ is evaluated inside the triangle (I, J, K), in the plane defined by the nodes I, J and K. Because the vectors $\mathbf{v}_{i,j}$ and $\mathbf{v}_{i,k}$, defined by points I and J and points I and K respectively (see Figure 1C–D), are linearly independent, the gradient can be written as the combination

$$\nabla V_i(t) = a(t)\, \mathbf{v}_{i,j} + b(t)\, \mathbf{v}_{i,k}$$

Using the boundary conditions

$$\begin{cases} \nabla V_i(t) \cdot \mathbf{v}_{i,j} &= V_j(t) - V_i(t) \\ \\ \nabla V_i(t) \cdot \mathbf{v}_{i,k} &= V_k(t) - V_i(t) \end{cases}$$

$a(t)$ and $b(t)$ can be evaluated, leading to an expression for the gradient

$$\nabla V_i(t) = \frac{1}{\Delta_{i,j,k}} \left((s_{i,k,k}\mathbf{v}_{i,j} - s_{i,j,k}\mathbf{v}_{i,k}) (V_j(t) - V_i(t)) + (s_{i,j,j}\mathbf{v}_{i,k} - s_{i,j,k}\mathbf{v}_{i,j}) (V_k(t) - V_i(t)) \right) \quad (25)$$

where

$$\begin{cases} s_{i,j,k} &= \mathbf{v}_{i,j}^t \mathbf{v}_{i,k} \\ \\ \Delta_{i,j,k} &= s_{i,j,j}s_{i,k,k} - s_{i,j,k}^2 = ||\mathbf{v}_{i,j} \wedge \mathbf{v}_{i,k}||^2 \end{cases} \quad (26)$$

Replacing the expression of the gradient in Equation (6) leads to

$$\begin{aligned} V_i(t+\delta t) &= V_i(t) + \frac{\delta t}{S_v C_m} \sum_{j \in \mathcal{N}_i} \sum_{k \in \mathcal{N}_i \cap \mathcal{N}_j} \alpha_{i,j,k} (V_j(t) - V_i(t)) + \beta_{i,j,k} (V_k(t) - V_i(t)) \\ &\quad - \frac{\delta t}{C_m} (I_{\text{ion},i}(t) - I_{\text{stim},i}(t)) \end{aligned}$$

where

$$\begin{cases} \alpha_{i,j,k} &= \frac{1}{\Omega_i \Delta_{i,j,k}} (s_{i,k,k}\mathbf{v}_{i,j}^t - s_{i,j,k}\mathbf{v}_{i,k}^t) \mathbf{D}^t (||\mathbf{u}_{i,j,k}|| \mathbf{n}_{i,j,k}) \\ \\ \beta_{i,j,k} &= \frac{1}{\Omega_i \Delta_{i,j,k}} (s_{i,j,j}\mathbf{v}_{i,k}^t - s_{i,j,k}\mathbf{v}_{i,j}^t) \mathbf{D}^t (||\mathbf{u}_{i,j,k}|| \mathbf{n}_{i,j,k}) \end{cases}$$

where $\mathbf{u}_{i,j,k}$ is the vector defined by points $G_{i,j,k}$ and $M_{i,j}$ (see Figure 1C–D). The terms in the two sums can then be grouped to have terms in $V_j(t) - V_i(t)$, leading to the coefficients

$$w_{i,j} = \sum_{k \in \mathcal{N}_i \cap \mathcal{N}_j} (\alpha_{i,j,k} + \beta_{i,k,j}) \quad (27)$$

where indices j and k are exchanged in the coefficient $\beta_{i,j,k}$. Making the appropriate substitutions, we obtain

$$V_i(t+\delta t) = V_i(t) + \frac{\delta t}{S_v C_m} \sum_{j \in \mathcal{N}_i} w_{i,j} (V_j(t) - V_i(t)) - \frac{\delta t}{C_m} (I_{\text{ion},i}(t) - I_{\text{stim},i}(t)) \quad (28)$$

and the weights $w_{i,j}$ are expressed as

$$w_{i,j} = \frac{1}{\Omega_i} \sum_{k \in \mathcal{N}_i \cap \mathcal{N}_j} \frac{1}{\Delta_{i,j,k}} \left(s_{i,k,k} \mathbf{v}_{i,j}^t - s_{i,j,k} \mathbf{v}_{i,k}^t \right) \mathbf{D}^t \left(||\mathbf{u}_{i,j,k}|| \ \mathbf{n}_{i,j,k} + ||\mathbf{u}_{i,k,j}|| \ \mathbf{n}_{i,k,j} \right)$$

($\Delta_{i,j,k} = \Delta_{i,k,j}$ and the scalar products verify $s_{i,j,k} = s_{i,k,j}$).

II. Evaluation of normals to the contour

The normal vector $\mathbf{n}$ to the contour can be expressed as the cross product between the vector tangent to the curve and the normal to the surface defined by the curve $\mathbf{n} = \mathbf{t} \wedge \mathbf{s}$ (see Figure 1A). Hence, for the surface defined by $(I, G_{i,j,k}, M_{i,j})$ and applied to the segment $[G_{i,j,k}, M_{i,j}]$ the normal vector to the curve is

$$\mathbf{n}_{i,j,k} = \gamma'_{i,j,k} \ \mathbf{u}_{i,j,k} \wedge \left(\mathbf{g}_{i,j,k} \wedge \mathbf{m}_{i,j} \right)$$

where $\mathbf{g}_{i,j,k}$ and $\mathbf{m}_{i,j}$ are the vectors given by points I and $G_{i,j,k}$ and points I and $M_{i,j}$, respectively (see Figure 1C–D) and where $\gamma'_{i,j,k}$ is a (positive) normalization coefficient. Using the double vector product (i.e. $(\mathbf{x} \wedge \mathbf{y}) \wedge \mathbf{z} = (\mathbf{x}^t \mathbf{z})\, \mathbf{y} - (\mathbf{y}^t \mathbf{z})\, \mathbf{x}$), the normal to the curve is given by

$$\mathbf{n}_{i,j,k} = \gamma'_{i,j,k} \left(-(\mathbf{g}_{i,j,k}^t \mathbf{u}_{i,j,k})\, \mathbf{m}_{i,j} + (\mathbf{m}_{i,j}^t \mathbf{u}_{i,j,k})\, \mathbf{g}_{i,j,k} \right)$$

We can then define this vector in terms of the vectors $\mathbf{v}_{i,j}$ and $\mathbf{v}_{i,k}$ using the fact that $\mathbf{m}_{i,j} = \frac{1}{2}\, \mathbf{v}_{i,j}$, that $\mathbf{g}_{i,j,k} = \frac{1}{3}\, \mathbf{v}_{i,j} + \frac{1}{3}\, \mathbf{v}_{i,k}$ and that $\mathbf{u}_{i,j,k} = \mathbf{m}_{i,j} - \mathbf{g}_{i,j,k}$ (see figure 1D). We obtain the simple expression

$$\mathbf{n}_{i,j,k} = \gamma_{i,j,k} \left((2 s_{i,k,k} - s_{i,j,k})\, \mathbf{v}_{i,j} + (s_{i,j,j} - 2 s_{i,j,k})\, \mathbf{v}_{i,k} \right)$$

where the normalization coefficient is expressed as

$$\gamma_{i,j,k} = \frac{1}{\Delta_{i,j,k}^{\frac{1}{2}} \left(s_{i,j,j} + 4 s_{i,k,k} - 4 s_{i,j,k} \right)^{\frac{1}{2}}}$$

Finally, exchanging the indices j and k in the equation above, we obtain the expression for $\mathbf{n}_{i,k,j}$.

III. Evaluation of linear combination of the normals

The length of the segment $[G_{i,j,k}, M_{i,j}]$ is given by

$$||\mathbf{u}_{i,j,k}|| = \frac{1}{6}\ (s_{i,j,j} + 4s_{i,k,k} - 4s_{i,j,k})^{\frac{1}{2}}$$

The linear combination is given by

$$||\mathbf{u}_{i,j,k}||\ \mathbf{n}_{i,j,k}\ +\ ||\mathbf{u}_{i,k,j}||\ \mathbf{n}_{i,k,j}\ =\ \frac{1}{2\,\Delta_{i,j,k}^{\frac{1}{2}}}\left(\left(s_{i,k,k} - s_{i,j,k}\right)\mathbf{v}_{i,j} + \left(s_{i,j,j} - s_{i,j,k}\right)\mathbf{v}_{i,k}\right) \tag{29}$$

IV. Evaluation of the surface Ω_i

The surface is the sum of sets of triangles (Figure 1B–D)

$$\Omega_i = \sum_{j\in\mathcal{N}_i}\ \sum_{k\in\mathcal{N}_i\cap\mathcal{N}_j} \Omega_{i,j,k}$$

where each set $\Omega_{i,j,k}$ defined by $(I, G_{i,j,k}, M_{i,j})$ is given by

$$\Omega_{i,j,k} = \frac{1}{2}\ \left|\left|\mathbf{g}_{i,j,k}\ \wedge\ \mathbf{m}_{i,j}\right|\right| = \frac{1}{12}\ ||\mathbf{v}_{i,k}\ \wedge\ \mathbf{v}_{i,j}||$$

V. Discretized Reaction–Diffusion Equation: General Case

Using the expression (29) the reaction–diffusion Equation (28) is given by

$$V_i(t+\delta t) = V_i(t) + \frac{\delta t}{S_v C_m}\sum_{j\in\mathcal{N}_i} w_{i,j}\ \left(V_j(t) - V_i(t)\right)\ -\ \frac{\delta t}{C_m}\left(I_{\text{ion},i}(t) - I_{\text{stim},i}(t)\right) \tag{30}$$

where the weights can be compactly expressed as

$$\begin{cases} w_{i,j} & = & \dfrac{1}{2\,\Omega_i}\displaystyle\sum_{k\in\mathcal{N}_i\cap\mathcal{N}_j} \dfrac{\left(s_{i,k,k}\,\mathbf{v}_{i,j}^t - s_{i,j,k}\,\mathbf{v}_{i,k}^t\right)\mathbf{D}^t\ \left(\left(s_{i,k,k} - s_{i,j,k}\right)\mathbf{v}_{i,j} + \left(s_{i,j,j} - s_{i,j,k}\right)\mathbf{v}_{i,k}\right)}{\Delta_{i,j,k}^{\frac{3}{2}}} \\ \\ s_{i,j,k} & = & \mathbf{v}_{i,j}^t\mathbf{v}_{i,k} \qquad s_{i,j,j} = ||\mathbf{v}_{i,j}||^2 \qquad s_{i,k,k} = ||\mathbf{v}_{i,k}||^2 \\ \\ \Delta_{i,j,k} & = & s_{i,j,j}s_{i,k,k} - s_{i,j,k}^2 = ||\mathbf{v}_{i,j}\ \wedge\ \mathbf{v}_{i,k}||^2 \\ \\ \Omega_i & = & \displaystyle\sum_{j\in\mathcal{N}_i}\ \sum_{k\in\mathcal{N}_i\cap\mathcal{N}_j} \Omega_{i,j,k} \qquad \text{where} \qquad \Omega_{i,j,k} = \frac{1}{12}\ ||\mathbf{v}_{i,j}\ \wedge\ \mathbf{v}_{i,k}|| \end{cases} \tag{31}$$

VI. Discretized Reaction–Diffusion Equation: Isotropic Case

In the case where the diffusion tensor is proportional to the identity $\mathbf{D} = \frac{1}{\rho}\mathbf{I}$ where ρ is the resistivity, Equation (30) can be written as

$$V_i(t+\delta t) = V_i(t) + \frac{\delta t}{\rho S_v C_m} \sum_{j \in \mathcal{N}_i} z_{i,j} \ (V_j(t) - V_i(t)) \ - \ \frac{\delta t}{C_m} \left(I_{\text{ion},i}(t) - I_{\text{stim},i}(t)\right) \tag{32}$$

where the weight are given by $z_{i,j} = \dfrac{1}{2\,\Omega_i} \displaystyle\sum_{k \in \mathcal{N}_i \cap \mathcal{N}_j} \frac{s_{i,k,k} - s_{i,j,k}}{\Delta^{\frac{1}{2}}_{i,j,k}}$. Recognizing that $s_{i,k,k} - s_{i,j,k} = \mathbf{v}^t_{k,j}\mathbf{v}_{k,i}$ and that $||\mathbf{v}_{i,j} \wedge \mathbf{v}_{i,k}|| = ||\mathbf{v}_{k,j} \wedge \mathbf{v}_{k,i}||$ we obtain

$$\left\{ \begin{array}{rcl} z_{i,j} & = & \dfrac{1}{2\,\Omega_i} \displaystyle\sum_{k \in \mathcal{N}_i \cap \mathcal{N}_j} \text{cotan}(\vartheta_{i,j,k}) \\ \\ \Omega_i & = & \displaystyle\sum_{j \in \mathcal{N}_i} \sum_{k \in \mathcal{N}_i \cap \mathcal{N}_j} \Omega_{i,j,k} \qquad \text{where} \qquad \Omega_{i,j,k} = \dfrac{1}{12} \ ||\mathbf{v}_{i,j} \wedge \mathbf{v}_{i,k}|| \end{array} \right. \tag{33}$$

where $\vartheta_{i,j,k}$ is the angle between $\mathbf{v}_{k,j}$ and $\mathbf{v}_{k,i}$ (since this angle is in $]0\ ,\ \pi[$ its sinus is strictly positive, see Figure 1D)).

References

[1] G. W. Beeler and H. Reuter, *Reconstruction of the action potential of ventricular myocardial fibers*, J. Physiol., vol. 268, pp. 177–210, 1977

[2] O. Blanc, N. Virag, J.-M. Vesin and L. Kappenberger, *A computer model of human atria with reasonable computation load and realistic anatomical properties*, IEEE Trans. on Biomedical Engineering, vol. 48, no. 11, pp. 1229–1237, November 2001

[3] M. Courtemanche, R. J. Ramirez and S. Nattel, *Ionic mechanism underlying human atrial action potential properties: insights from a mathematical model*, AJP Heart and Circ. Physiol., vol. 44, no. 1, pp. H301–H321, July 1998

[4] D. DiFrancesco and D. Noble, *A model of cardiac electrical activity incorporating ionic pumps and concentration changes*, Phil. Trans. Roy. Soc. London B, vol. 307, pp. 353–398, 1985

[5] R. A. FitzHugh, *Impulses and physiological states in theoretical models of nerve membrane*, Biophysics Journal, vol. 1, pp. 445–466, 1961

[6] J. Garrigues, *La méthode des éléments finis*, Cours de l'école supérieure de mécanique de Marseille, Janvier 2001

[7] P.L. George and H. Borouchaki, *Delaunay triangulation and meshing: application to finite elements*, Hermès, Paris, 1998

[8] D. B. Geselowitz, R. C. Barr, M. S. Spach and W. T. Miller 3rd, *The impact of adjacent isotropic fluids on electrograms from anisotropic cardiac muscle. A modeling study*, Circulation Research, vol. 51, no. 5, pp. 602–613, November 1982

[9] D. B. Geselowitz, *On the theory of electrocardiogram*, Proceedings of the IEEE, vol. 77, no. 6, pp. 857–875, June 1989

[10] K. Gima and Y. Rudy, *Ionic Current Basis of Electrocardiographic Waveforms: A Model Study*, Circulation Research, vol. 90, no. 8, pp. 889–896, May 2002

[11] F. X. Giraldo, *Lagrange–Galerkin methods on spherical geodesic grids*, Journal of Computational Physics, vol. 136, no. 1, pp. 197–217, September 1997

[12] G. H. Golub and C. F. Van Loan, *Matrix computations*, The John Hopkins University Press, Baltimore, 1987

[13] D. M. Harrild, C. S. Henriquez, *A finite volume model of cardiac propagation*, Annals of Biomedical Engineering, vol. 28, no. 2, pp. 315–334, March–April 1997

[14] D. M. Harrild, C. S. Henriquez, *A computer model of normal conduction in the human atria*, Circulation Research, vol. 87, pp. 25e–36e, September 2000

[15] C. S. Henriquez and A. A. Papazoglou, *Using computer models to understand the roles of tissue structure and membrane dynamics in arrhythmogenesis*, Proc. of the IEEE, vol. 84, no. 3, pp. 334–354, March 1996

[16] I. J. Le Grice, B. H. Smail and P. J. Hunter, *Myocardial activation by threshold modeling with an anatomically accurate finite element model*, Proc. of the Biomedical Engineering Society, 1992

[17] P. Levran, *Simulation de cellules cardiaques par automates cellulaires*, rapport de diplôme, département d'électricité, Ecole Polytechnique Fédérale de Lausanne, 1999–2000

[18] C. Luo and Y. Rudy, *A dynamic model of the cardiac ventricular action potential, I: simulations of ionic currents and concentration changes*, Circulation Research, vol. 74, pp. 1071–1096, June 1994

[19] A. Nygren, C. Fiset, L. Firek, J. W. Clark, D. S. Lindblad, R. B. Clark and W. R. Giles, *Mathematical model of an adult human atrial cell. The role of K+ currents in repolarization*, Circulation Research, vol. 82, pp. 63–81, January 1998

[20] I. Ohnaka and T. Fukusako, *Finite element method and a matrix method in transient heat–conduction problems*, Sixth International Heat Transfer Conference, Toronto, vol. 3, pp. 251, 1988

[21] R. Plonsey and R. C. Barr, *Bioelectricity: a quantitative approach*, chap. 8, 2nd edition, Kluwer academic, Plenum publishers, New York, 2000

[22] M. Rappaz and M. Bellet and M. Deville, *Modélisation numérique en science et génie des matériaux*, Presses Polytechniques et Universitaires Romandes, 1998

[23] J. M. Rogers and A. D. McCulloch, *A collocation–Galerkin finite element model of cardiac action potential*

propagation, IEEE trans. on Biomedical Engineering, vol. 41, no. 8, pp. 743–757, August 1994

[24] D. J. Rose, H. Shao and C. S. Henriquez, *Discretization of anisotropic convection–diffusion equations, convective M–matrices and their iterative solution*, VLSI Design, vol. 10, no. 4, pp. 485–529, 2000

[25] F. B. Sachse, C. Werner and G. Seeman, *Simulation of cardiac electrophysiology and electrocardiography*, in Computer Simulation and Experimental Assessment of Cardiac Electrophysiology, pp. 97–104, N. Virag, O. Blanc, L. Kappenberger Editions, Futura Publishing, Armonk, New–York, 2001

[26] M. S. Spach and J. M. Kootsey, *Relating the sodium current and conductance to the shape of transmembrane and extracellular potentials by simulation: effects of propagation boundaries*, IEEE trans. on Biomedical Engineering, vol. 32, no. 10, pp. 743–755, October 1985.

[27] R. S. Varga, *Matrix iterative analysis*, 2nd edition, Springer Verlag, New–York, 2000

[28] N. Virag, J. M. Vesin and L. Kappenberger, *Electrocardiogram simulation with a ionic current computer model of the cardiac tissue*, Proc. of the 20th annual IEEE Int. Conf. on Engineering in Medicine and Biology Society, pp. 32–35, Hong Kong, Oct. 29–Nov. 1, 1998

[29] C. W. Zemlin, H. Herzel, S.Y. Ho and A. Panvilov, *A realistic and efficient model of excitation propagation in the human atria*, in Computer Simulation and Experimental Assessment of Cardiac Electrophysiology, pp. 29–34, N. Virag, O. Blanc, L. Kappenberger Editions, Futura Publishing, Armonk, New–York, 2001

List of Figures

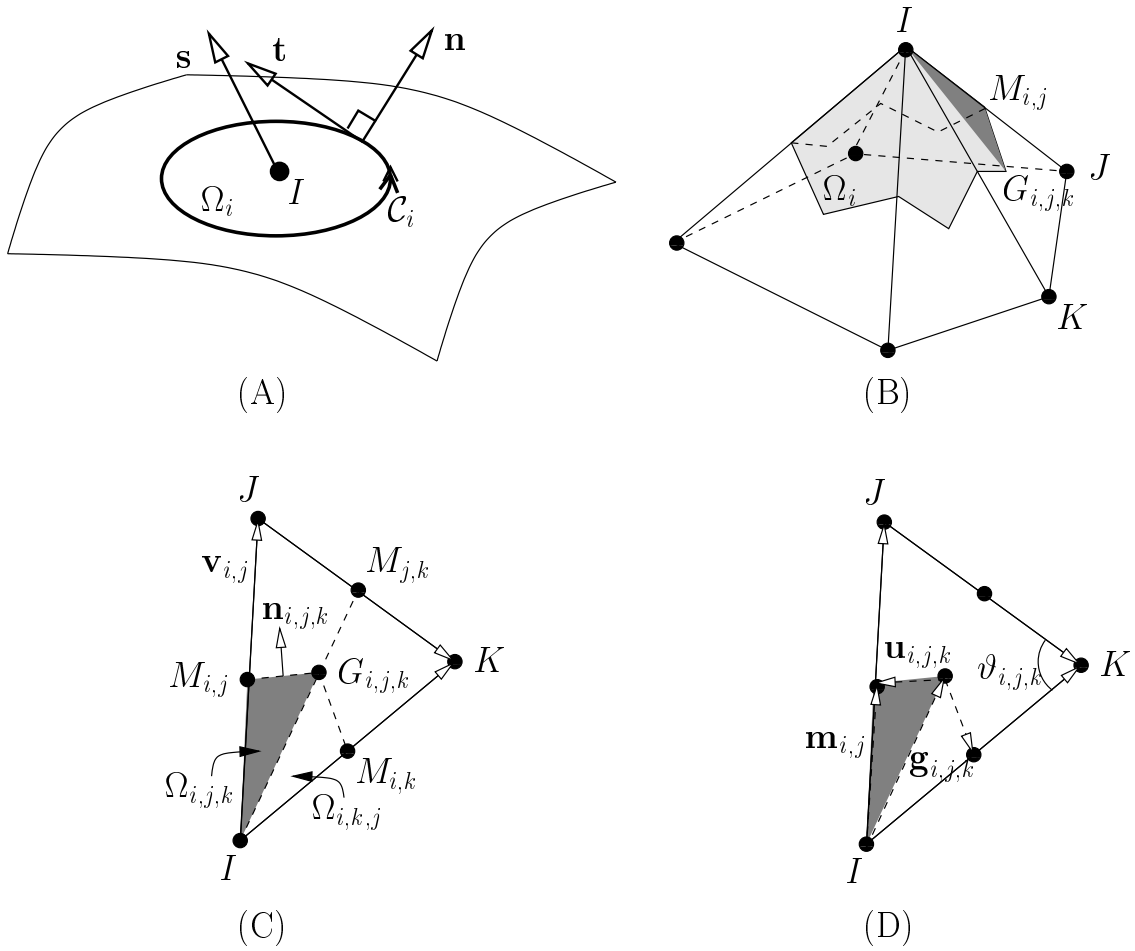

Fig. 1. (A): for a fixed point I, $\mathcal{C}_i$ denotes a contour surrounding I, Ω_i denotes the surface defined by the contour, the normal vector to the surface is then denoted $\mathbf{s}$, the tangent vector is denoted $\mathbf{t}$ and the "normal–tangent" vector to the contour is denoted $\mathbf{n}$. (B): schematic description of the contour around node I for a triangular mesh and the associated surface Ω_i; The contour is the union of the segment defined by the midpoint of each vertex and the gravity center of each triangle; The surface if then the union of each sub–surface. (C) and (D): definition of the piece of the contour in each triangle sharing node I. Vectors $\mathbf{v}_{i,j}$, $\mathbf{v}_{i,k}$ and $\mathbf{v}_{j,k}$ are the vectors defined through points I and J, I and K, J and K respectively; $G_{i,j,k}$ denotes the gravity center of the triangle (I,J,K); $M_{i,j}$ and $M_{i,k}$ denote the midpoints of segments $[I,J]$ and $[I,K]$ respectively; Hence, the normal vectors to segment $[G_{i,j,k},M_{i,j}]$ and segment $[G_{i,j,k},M_{i,k}]$ are respectively $\mathbf{n}_{i,j,k}$ and $\mathbf{n}_{i,k,j}$; The sub–surfaces defined by triangle $(I,G_{i,j,k},M_{i,j})$ and triangle $(I,G_{i,j,k},M_{i,k})$ are respectively $\Omega_{i,j,k}$ and $\Omega_{i,k,j}$. The intermediate vector we use in appendix are $\mathbf{m}_{i,j}$ and $\mathbf{m}_{i,k}$ defined using I and $M_{i,j}$, I and $M_{i,k}$ respectively; Vectors $\mathbf{u}_{i,j,k}$ and $\mathbf{u}_{i,k,j}$ are given by $G_{i,j,k}$ and $M_{i,j}$, $G_{i,j,k}$ and $M_{i,k}$ respectively; Vector $g_{i,j,k}$ is defined by points I and $G_{i,j,k}$; At last the angle $\vartheta_{i,j,k}$ denotes the angle between vectors $\mathbf{v}_{k,i}$ and $\mathbf{v}_{k,j}$.

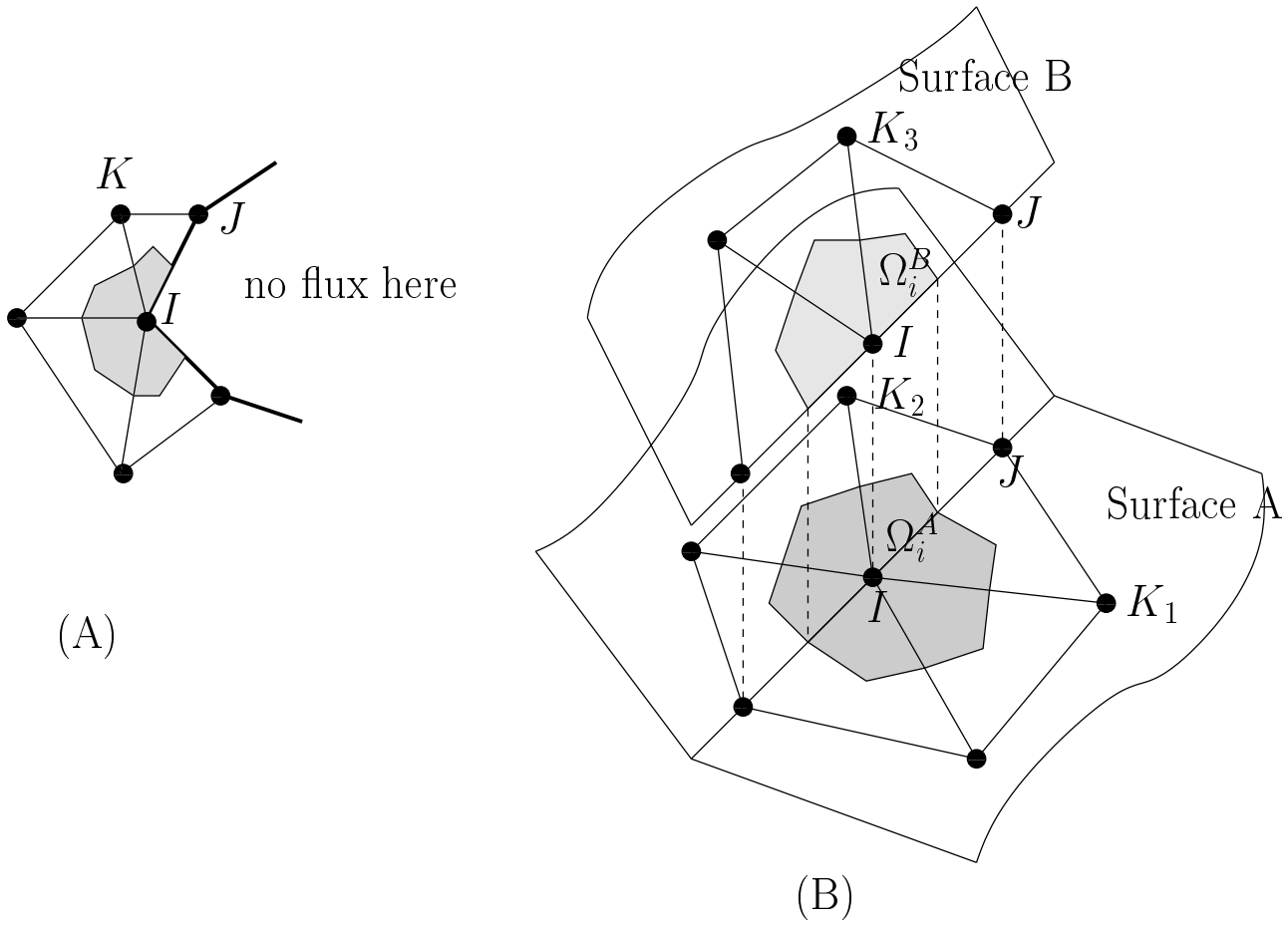

Fig. 2. Schematics of the special cases of (A) holes and (B) connection of two surfaces.

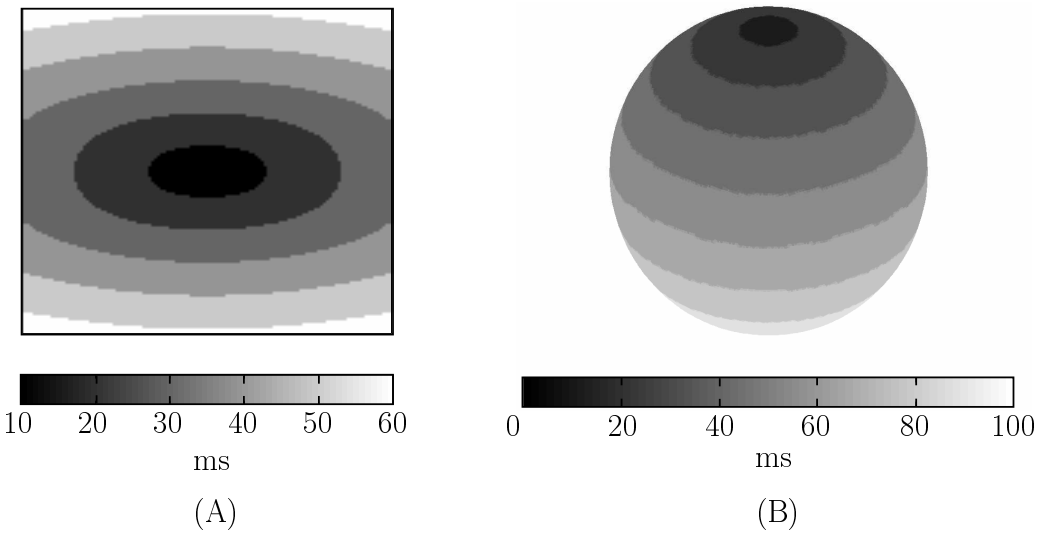

Fig. 3. Isochrones for elementary surfaces; (A) case of the anisotropic square sheet of tissue (5 cm by 5 cm) for the described simulation; (B) case of isotropic the sphere of radius of 3 cm for the described simulation.

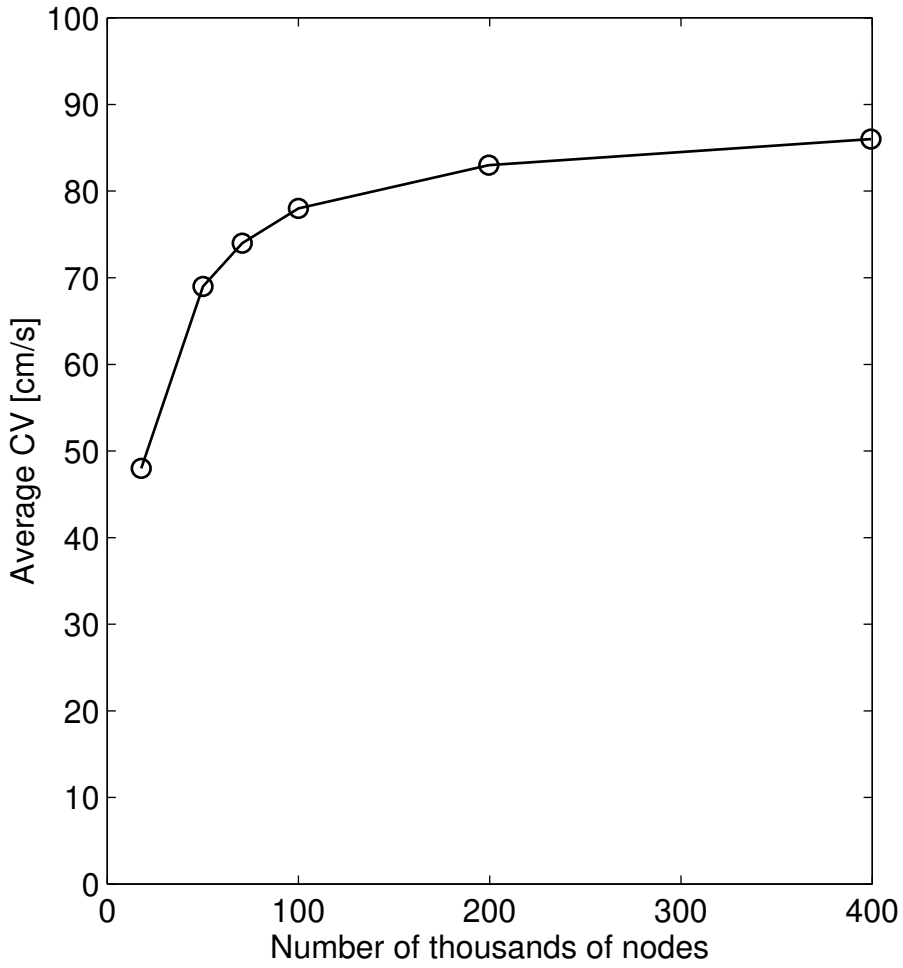

Fig. 4. Average conduction velocity (CV) measured during an impulse propagation on the atrial surface meshed with different spatial resolutions: 17'000, 50'000, 100'000, 200'000, 400'000 nodes with a mean distance between nearest neighbors of approximately 1000, 600, 400, 300, 200 μm respectively.

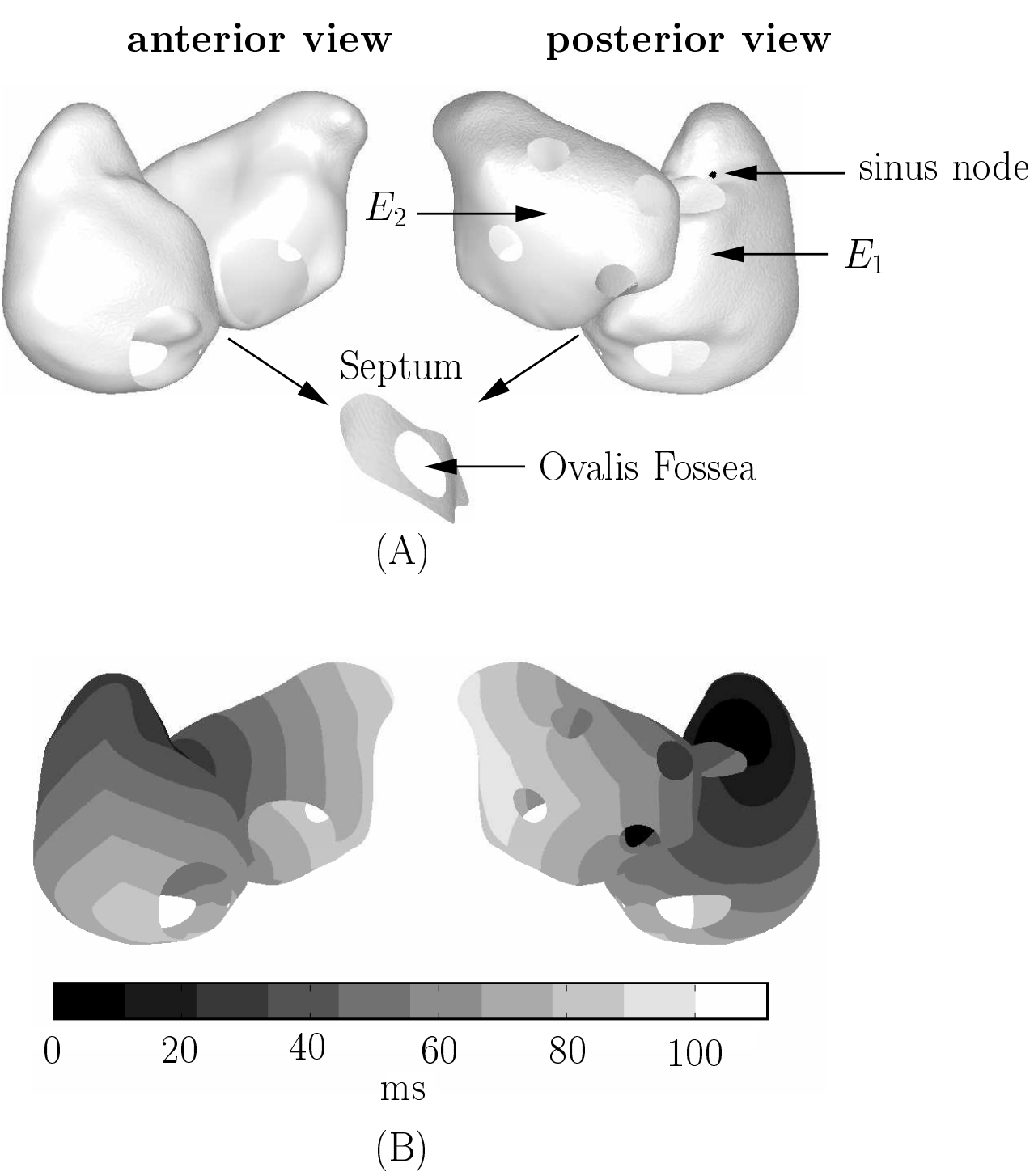

Fig. 5. (A): Mesh of the atrium. The holes corresponding to the insertion sites of the vessels and valves (4 pulmonary veins, superior and inferior venas cava, tricuspid and mitral valves, sinus coronary) are shown. In addition, the septum (junctions of several surfaces) and the fossea ovalis (that can be modeled as a hole if it does not diffuse) are represented separately. The black dot indicates the location of the sinus node. E_1 and E_2 indicate the location of the simulated recording electrodes. (B): Sinus node stimulation: propagation isochrones.

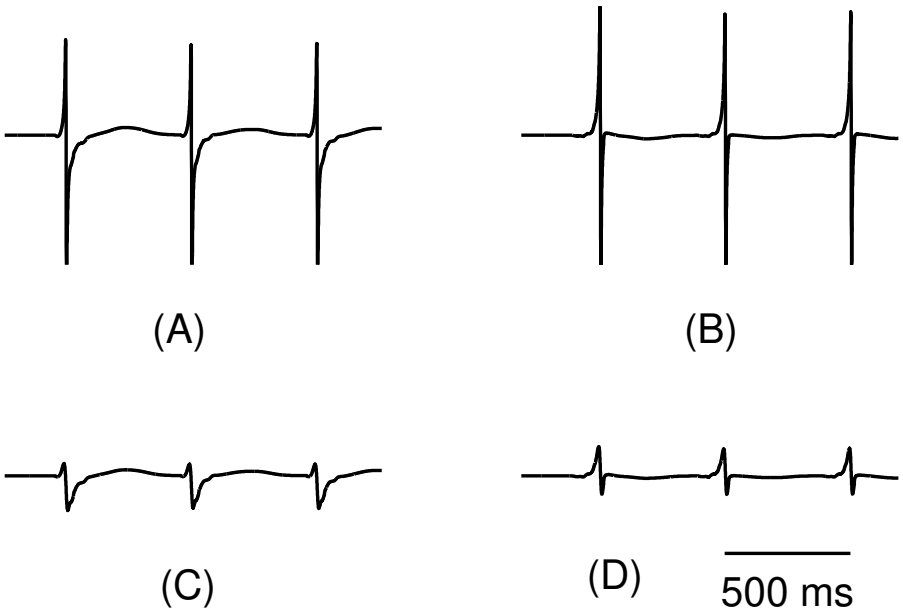

Fig. 6. Simulated unipolar electrograms during normal sinus rythm. (A) and (C) Electrode located at position E_1 (see Figure 5A), respectively at 1 mm and 5 mm from the surface; (B) and (D) Electrode located at position E_2 (see Figure 5A), respectively at 1 mm and 5 mm from the surface.

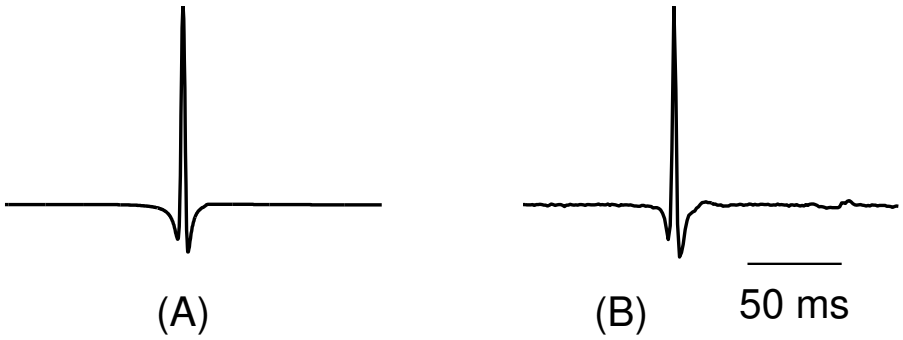

Fig. 7. (A) Simulated bipolar electrogram (normalized amplitude) measured at position E_1 (see Figure 5A), at 1 mm from the surface. (B) Clinical bipolar electrogram (normalized amplitude) recorded in a right human atrium during routine intracardiac mapping. In both cases the distance between the electrodes is 2 mm.